arXiv:astro-ph/0204181v1 10 Apr 2002

Mg II Absorption Lines in z=2.974 Damped Lyman-α system toward Gravitationally Lensed QSO APM 08279+5255: Detection of Small-scale Structure in Mg II Absorbing Clouds[1]

Naoto Kobayashi, Hiroshi Terada, Miwa Goto

Subaru Telescope, National Astronomical Observatory Japan, 650 North A'ohoku Place, Hilo, HI 96720

naoto@naoj.org

and

A. T. Tokunaga

Institute for Astronomy, University of Hawaii, 2680 Woodlawn Drive, Honolulu, HI 96822

ABSTRACT

$1.02-1.16\,\mu$m spectra ($\lambda/\Delta\lambda \sim 7{,}000$) of the gravitationally lensed QSO APM 08279+5255 at z_{em}=3.911 were obtained during the commissioning run of IRCS, the $1-5\,\mu$m near-infrared camera and spectrograph for the Subaru 8.2 m Telescope. Strong Mg II doublet $\lambda\lambda$2976,2800 and Fe II λ2600, Fe II λ2587 absorption lines at z_{abs}=2.974 were clearly detected in the rest-frame UV spectra, confirming the presence of a damped Lyman-α system at the redshift as suggested by Petitjean et al. Also Mg I λ2853 absorption line is probably detected. An analysis of the absorption lines including velocity decomposition was performed. This is a first detailed study of Mg II absorption system at high redshift (z > 2.5) where the Mg II doublet shifts into the near-infrared in the observer's frame.

The spectra of the lensed QSO pair A and B with 0″.38 separation were resolved in some exposure frames under excellent seeing condition. We extracted the Mg II doublet spectra of A and B separately. Although three velocity components (v$\sim$-28, +5, +45 km s^{-1}) are known to exist in this Mg II system (Petitjean et al.), the v$\sim$+45 km s^{-1} absorption line was *not* detected toward source

---

[1]Based on data collected at Subaru Telescope, which is operated by the National Astronomical Observatory of Japan.

B, showing that the $+45$ km s^{-1} Mg II cloud lies only in the line of sight to the source A. Our results suggests that the size of the Mg II absorbing clouds is as small as 200 pc, which corresponds to the separation of A and B at the redshift of the absorber. This is the first direct detection of the small-scale structure of Mg II clouds at high-redshift, confirming the estimated cloud sizes from photoionization model by Churchill and Charlton.

Subject headings: quasars: absorption lines – quasars: individual (APM 08279+5255) – gravitational lensing – intergalactic medium – galaxies: formation

1. Introduction

The gravitationally lensed QSO APM 08279+5255 (z_{em}=3.911) has been given much attention since its discovery by Irwin et al. (1998). There are two major gravitationally lensed images "A" and "B" with a separation of $0''.38$ and flux ratio of f_B/f_A=0.77 (Ibata et al. 1999). Third faint image "C" was also reported by Ibata et al. (1999) between A and B, with a separation of A-C=$0''.15$ and with the flux ratio of f_C/f_A=0.18.

Petitjean et al. (2000) suggested a probable damped Lyman-α (DLA) system at z_{abs}=2.974 which has $19.8 < \log N(HI) \ [cm^{-2}] < 20.3$ from data obtained with Keck HIRES (Ellison et al. 1999a,b). The low metallicity ([X/H] $\sim$ -2.3) derived from weak metal lines (Fe, Al, Si, C and O) suggest a very small dust amount in the cloud. Thus, this DLA system is an important object which supports the idea that there may be a metallicity evolution of DLA in z $>$ 3 (see discussions in Petitjean et al. 2000, Pettini et al. 1997, 1999).

Another interest of the DLA system is any difference of absorption features in the line of sight to the images A, B, and C. The small separation of A-B, which is estimated at $\sim$ 200h$_{75}^{-1}$ pc (Petitjean et al. 2000), gives us a unique opportunity to investigate small ($<$ 1 kpc) spatial structure of DLA systems at high-z. A systematic study of small-scale structure of high-ionization gas (C IV) at high redshift was performed by Rauch et al. (2001) by observing a number of gravitationally lensed QSOs with Keck HIRES. They found C IV clouds do not seem to have small scale structure for regions smaller than a few hundred parsecs. Lopez et al. (1999) also show that O VI is spread out over large scales.

However, there is a strong interest in lower-ionization clouds since they trace the neutral hydrogen gas (e.g., Wolfe & Prochaska 2000a) which should be the source of star-forming molecular clouds. If high-z DLAs are the progenitor of the present-day disk galaxies (e.g., Storrie-Lombardi & Wolfe 2000 and references therein), the spatial-structure of low-ionization clouds gives us insights into how the "protogalaxies" are assembled from building

blocks (e.g., Haehnelt, Steinmetz, & Rauch 1998, Wolfe & Prochaska 2000b). Although Rauch et al. (1999) found a strong variation of low-ionization C II and Si II absorption at z = 3.538 along two sight-lines separated by only $26h_{50}^{-1}$ pc for Q1422+231 (z_{em} = 3.628), it cannot be excluded that the system is somehow associated with the quasar as discussed by Rauch et al. (1999) because the velocity difference between the QSO and the system is only 6000 km s^{-1}.

Mg II absorption lines are one of the most promising probes for studying such low-ionization clouds (Churchill & Vogt 2001). The Mg II $\lambda\lambda$ 2796,2803 doublet absorption lines are most noted as being associated with galaxies (Bergeron & Boissé 1991; Steidel, Dickinson & Persson 1994) and its kinematics for low to intermediate redshift DLAs are comprehensively studied (Churchill & Vogt 2001 and references therein). However, there has been no detailed Mg II absorption line study for high-redshift (z > 2.5) DLAs because Mg II doublet absorption line shifts into the near-infrared ($\lambda > 1\,\mu$m) in the observer's frame and until recently there has been no capability of high-resolution near-infrared spectroscopy with a large aperture telescope.

Here we present near-infrared $1.02-1.16\,\mu$m spectra of APM 08279+5255 with $40-45$ km s^{-1} spectral resolutoin, obtained with the near-infrared spectrograph IRCS at the Subaru Telescope. In this rest-frame UV spectra, we have detected Mg II doublet and Fe II absorption lines originated from the DLA system at z_{abs}=2.974. Although future higher resolution (< 10 km s^{-1}) study is in order, the present data gives us a variety of information on the DLA system with reasonable signal-to-noise. Also, a difference of the Mg II absorption lines between the images A and B was clearly detected in our spectrum under excellent seeing condition. In the following, §2 describes the observation and §3 describes the results and preliminary analysis.

2. Observations

Near-infrared $1.02-1.18\,\mu$m spectra of APM 08279+5255 were obtained on 11 January 2001 UT during the scientific commissioning run of IRCS, a $1-5\,\mu$m near-infrared camera and spectrograph at the Japanese Subaru 8.2m telescope (Tokunaga et al. 1998, Kobayashi et al. 2000) on Mauna Kea, Hawaii. We used the cross-dispersed Echelle mode of IRCS, which provides a spectral resolution of 15 km s^{-1} ($\lambda/\Delta\lambda \sim 20,000$) with a 0.15-arcsec slit. The pixel scale is 0.075-arcsec per pixel in spatial direction and about 7.5 km s^{-1} per pixel in the dispersion direction. The entire IRCS "zJ-band" ($1.02-1.18\,\mu$m) was covered simultaneously in one exposure with the cross-disperser used in order 6 and the echelle in order 48 to 55. Although seeing was good throughout the observing time (0″.3 to 0″.55 in zJ-band), we used

a wider slit (0″6) to maximize the throughput of the slit. Thus, the spectral resolution was determined by the seeing size and the resultant spectral resolution was $40 - 45$ km s^{-1} ($\lambda/\Delta\lambda \sim 7{,}000$) in the observed wavelength range.

The slit length was 3.8-arcsec and the slit angle was set to P.A. = 32° so that both the lensed images A and B are in the slit. The object was nodded along the slit by about 2″ after a 300 sec exposure for sky-background and dark subtraction. Because of the fine pixel scale needed for adaptive optics images and the high spectral resolution, it is impossible to reach the background-limit within a single exposure ($300-600$ sec) which was less than the time-variation of the sky OH-emission. Four sets of data were obtained, resulting in a total exposure time of 2400 sec. Spectra of bright telluric standard stars (HR 4905: A0p, HR 5191: B3V) at similar airmass were obtained in similar fashion, but only HD 5191 was used in the following analysis because HD 4905 had several unidentified stellar absorption lines.

The obesrving log is shown in Table 1. Although we started the observing right after focusing the secondary mirror of the telescope, the image quality had gradually changed during the observing due to a seeing change from 0″30 to 0″55 in zJ-band in an hour. Thus, we had good image quality only for the first few frames, in which we could resolve the images A and B with 0″38 separation in the echellogram (discussed in detail in §3.2).

All the data were reduced following standard procedures using the IRAF[2] noao.imred.echelle package: sky subtraction (subtraction of two frames), flat-fielding (halogen lamp with an integrating sphere), and aperture extraction. Argon lamp spectra which were taken at the end of the observing night were used for wavelength calibration. Using atmospheric absorption lines in the object and standard spectra, we confirmed that the pixel shift along the dispersion direction was less than 1-pixel throughout the observing time including the calibration.

3. Results and Discussions

3.1. Mg II and Fe II Absorption Lines

Figure 1 shows $1.02-1.16\,\mu$m spectrum of APM 08279+5255. The raw spectrum was smoothed to 3 pixels (22.5 km s^{-1}) with a boxcar function for better signal-to-noise. Strong Mg II $\lambda\lambda$2796,2803 absorption lines as well as Fe II λ2587 and λ2600 absorption lines from

---

the DLA system at $z_{abs} = 2.974$ are clearly seen in this spectrum. Mg I $\lambda2853$ absorption line is probably detected at the expected wavelength for the redshift, but qutantitative numbers for this line should be taken with cautions because of the strong atmospheric absorption lines at $1.12 - 1.15\,\mu$m.

The detected absorption lines are summarized in Table 2. Because the equivalent width ratio[3] W(2796)/W(2803) is about 1.4, the Mg II $\lambda2796$ absorption line should have saturated velocity components. Fe II $\lambda2600$ may be also saturated judging from the relatively deep absorption of our low resolution spectrum. Petitjean et al. (2000) showed that the Fe II $\lambda1608$ absorption line has 40% absorption at the core of the line with $\sim$8 km s^{-1} resolution. Because the oscillator strength of Fe II $\lambda2600$ (f=0.2239; Morton 1991) is about three times larger than that of Fe II $\lambda1608$ (f=0.064408; Savage & Sembach 1996), the Fe II $\lambda2600$ line is most likely partly saturated.

The column density and metallicity of Fe II, Mg II, and Mg I estimated from the equivalent widths are also summarized in Table 2. In view of the large equivalent widths, Fe II $\lambda2600$, Mg II $\lambda\lambda2796,2803$ lines should be saturated (see examples in Churchill et al. 1999, Churchill et al. 2000a and Churchill et al. 2000b). Thus, the estimated column densities for those lines are a lower-limit. We assumed that Fe II $\lambda2587$, Mg I $\lambda2583$ lines are not saturated. The following equation for optically thin limit from Savage and Sembach (1996) was used for estimating the column densities: $N[\mathrm{cm}^{-2}] = 1.13 \times 10^{17}$ W[mÅ] / (f λ^2[Å]), where λ is rest wavelength, f is oscillator strength, and W is equivalent width of the line. The estimated metallicity of Fe II and Mg II in Table 1 is consistent with the result for other metal lines in Petitjean et al (2000), supporting their conclusion that the DLA system has quite low-metallicity ([X/H] $\sim$ -2.0 $-$ -2.5) and may suggest the system's "young" nature compared to lower-redshift DLA systems (Petitjean et al. 2000).

Figure 2 shows the line profile of Mg II doublet and Fe II $\lambda2600$ absorption lines on a velocity scale with the origin at z_{abs}=2.9740. In our spectrum, all three lines show two major velocity components at v $\sim$ -10 km s^{-1} (hereafter "main component") and $\sim$ +45 km s^{-1} (hereafter "subcomponent"). Gaussian fit to the two components was performed for Mg II doublet and Fe II $\lambda2600$ using IRAF *splot* task (Table 2). We did not use Voigt profile fitting because the spectral resolution is not high enough to extract high precision information. We performed a simple Gaussian fitting with maximum two components and the decomposition of absorption lines is only approximate. The fitted Gaussian FWHM suggests that the main component has a velocity spread no more than 80 km s^{-1}. The main component should be

---

[3]The ratio of the Mg II doublet equivalent width (W(2796)/W(2803)) should be 2 for non-saturated case and 1 for fully-saturated case.

saturated for both Mg II $\lambda\lambda$ 2796, 2803 and probably for Fe II λ 2600. The subcomponent is weaker, but the equivalent width ratio of the Mg II doublet is $W_{sub}(2796)/W_{sub}(2803) \lesssim$ 1 and this may suggest that the subcomponent is saturated. The relatively large equivalent width ($W_{rest} \sim 0.1$Å) also suggests that at least Mg II λ2796 line is saturated (Churchill & Vogt 2001).

Petitjean et al (2000) identified three major velocity components at around -28 km s^{-1}, +5 km s^{-1}, and +45 km s^{-1} for 10 metal absorption lines in Keck HIRES data with velocity resolution of $\sim$8 km s^{-1}. Because Petitjean et al. 2000 does not list the velocity of the three components, we estimated the velocity from the vertical lines in their Figure 12. An additional velocity components may be present between -28 and +5 km s^{-1} components in their Figure 12 and, in particular, it is clearly seen in Al II λ1670 absorption spectrum. With lower spectral resolution, three velocity components (-28 km s^{-1}, -10 km s^{-1}, +5 km s^{-1}) should be blended and the peak position would shift to about -10 km s^{-1}. Thus, we identified our "main component" as the mixture of those three components in Petitjean et al. (2000). Their +45 km s^{-1} component coincides with our "subcomponent" seen in Mg II $\lambda\lambda$ 2796,2803 and Fe II λ2600 absorption lines. The identification is summarized in Table 3.

3.2. Spatially-resolved Spectra of Images A and B

Because the seeing was less than $0\rlap{.}''4$ at the beginning of observing, two images of the gravitationally lensed QSO, A and B with $0\rlap{.}''38$ separation, were resolved in the first three frames of 300 sec exposure (see §2 and Table 1). In all the three frames it was noticed that only image A has the "subcomponent" at +45 km s^{-1} while both have the "main component" in common at around -10 km s^{-1} (Figure 3). We combined those three frames and extracted spectra of A and B separately to examine any difference of the DLA absorption lines. Extracted spectra for A and B (Figure 4) also show the difference clearly.

Figure 5 shows the cross-cuts of the combined spectrum in spatial direction. The light grey line shows continuum profile on both sides of the Mg II absorption lines while dark grey line shows the profile at +45 km s^{-1} component. In this plot it is clearly shown that image A has significantly less flux at +45 km s^{-1} than at the continuum while image B has almost similar flux as at the continuum. A slight dip of the dark grey line near image C may suggest that the flux from image C also sigfinicantly decreased at +45 km s^{-1}. However, that is not clear because the spatial resolution ($\sim 0\rlap{.}''35$) is not enough for the small separation between A and C ($0\rlap{.}''15$). Therefore, we performed a gaussan fitting to the spatial profiles for Mg II λ2796 line (Figure 6). The continuum profile was fitted well with the combination of three gaussians at A, B, and C positions with the exact flux ratio as in Ibata et al. (1999). The

profile at $+45$ km s^{-1} was well fitted similarly with 50% less flux for A and 80% less flux for C (see black lines in the right panel). We tried to fit the $+45$ km s^{-1} profile without decreasing the C flux, but could not reproduce the dip at C-position well (see grey lines in the same panel). This result suggests that the $+45$ km s^{-1} component is present also in image C and significantly decrease the flux from C. However, in view of the uncertainty of the profile data (see e.g., the difference of two continuum profiles for Mg II 2796 line, which indicates the uncertainty of the profile in Figure 5), the fitting results for image C should be treated with caution. In a summary, we conclude that: (1) image B does not have any absorption from the $+45$ km s^{-1} component, (2) image A has $\sim$50% absorption from the $+45$ km s^{-1} component, (3) image C may have very strong absorption from the $+45$ km s^{-1} component.

Because the estimated distance between images A and B of APM 08279+5255 is only $200h_{75}^{-1}$ pc at the redshift of the z=2.974 DLA system (Petitjean et al. 2000), our results suggest that there is a small-scale structure (< 200 pc) in the DLA system. Figure 5 shows that the fractional change in column density of the subcomponent from A to B is almost 1, suggesting a sharp cut-off of this subcomponent. If the strong absorption from the subcomponent truly exists in C as suggested from the above analysis, it sets a lower limit on the size of the absorbing cloud of $\sim 80h_{75}^{-1}$ pc, which corresponds to the separation of A and C ($= 0\rlap{.}''15$). For high-ion C IV clouds, Rauch et al. (2001) found that they are mostly featureless on scales below ~ 300 pc and the fractional change in column density is mostly less than 0.2 for such small scales (see Figures 8 & 9 in Rauch et al. 2001). Our results suggest that low-ionization clouds may have finer structure than high-ionization clouds at high-z, but a more systematic study is needed to address this point.

The velocity difference of the subcomponent to the main component is about 50 km s^{-1} and the subcomponent is classified as "moderate" velocity subsystem in the classification of kinematic Mg II subsystems by Churchill & Vogt (2001). The velocity of the subsystem and the equivalent width is well within the ranges for low to intermediate redshift DLAs studied by Churchill & Vogt (2001). They found that the high or moderate velocity subsystem is probably *not* higher redshift analogues to the Galactic high velocity clouds (HVCs) in the halo or intergalactic space because the H I column density of the substems is too low for HVCs. Churchill & Charlton (1999) found that the Mg II subsystems are more like compact clouds which are embedded in extended highly ionized gas like Galactic coronae. From the ionization modeling of those clouds, they inferred the masses and sizes of the Mg II clouds at $\sim$ few $\times$ 10 M$_\odot$ and $\sim$ few $\times$ $10 - 100$ pc. Their inferred size is consistent with our results for the subsystem of the DLA at z$_{abs}$ =2.974 ($\lesssim 200$ pc). Although more systematic study is in order, our result presents the first glimpse of small-scale structure of low-ionization Mg II clouds in a DLA system at high redshift.

REFERENCES

Bergeron, J. & Boissé, P. 1991, A&A, 243, 344

Churchill, C. W. & Vogt, S. S. 2001, AJ, 122, 679

Churchill, C. W., Mellon, R. R., Charlton, J. C., Jannuzi, B. T., Kirhakos, S., Steidel, C. C., & Schneider, D. P. 2000, ApJS, 130, 91

Churchill, C. W., Mellon, R. R., Charlton, J. C., Jannuzi, B. T., Kirhakos, S., Steidel, C. C., & Schneider, D. P. 2000, ApJ, 543, 577

Churchill, C. W. & Charlton, J. C. 1999, AJ, 118, 59

Ellison, S. L., Lewis, G. F., Pettini, M., Chaffee, F. H., & Irwin, M. J. 1999a, ApJ, 520, 456

Ellison, S. L., Lewis, G. F., Pettini, M., Sargent, W. L. W., Chaffee, F. H., Foltz, C. B., Rauch, M., & Irwin, M. J. 1999b, PASP, 111, 946

Haehnelt, M. G., Steinmetz, M., & Rauch, M. 1998, ApJ, 495, 647

Ibata, R.A., Lewis, G.F., Irwin, M.J., Leha'r, J., & Totten, E.J. 1999, AJ, 118, 1922

Irwin, M.J., Ibata, R.A., Lewis, G.F., & Totten, E.J. 1998, ApJ, 505, 529

Kobayashi, N. et al. 2000, Proc. SPIE, 4008, 1056

Lopez, S., Reimers, D., Rauch, M., Sargent, W. L. W., & Smette, A. 1999, ApJ, 513, 598

Lord, S. D. 1992, NASA Technical Memorandum 103957

Morton, D.C. 1991, ApJS, 77, 119

Petitjean, P., Aracil, B., Srianand, R., & Ibata, R. 2000, A&A, 359, 457

Pettini, M., Ellison, S. L., Steidel, C. C., & Bowen, D. V. 1999, ApJ, 510, 576

Pettini, M., Smith, L. J., King, D. L., & Hunstead, R. W. 1997, ApJ, 486, 665

Rauch, M., Sargent, W.L.W., & Barlow, T.A. 2001, ApJ, 554, 823

Rauch, M., Sargent, W.L.W., & Barlow, T.A. 1999, ApJ, 515, 500

Savage, B.D. & Sembach, K.R. 1996, ARA&A, 34, 279

Steidel, C. C., Dickinson, M., & Persson, S. E. 1994, ApJ, 437, L75

Storrie-Lombardi, L. J. & Wolfe, A. M. 2000, ApJ, 543, 552

Tokunaga, A. T. et al. 1998, Proc. SPIE, 3354, 512

Wolfe, A. M. & Prochaska, J. X. 2000a, ApJ, 545, 603
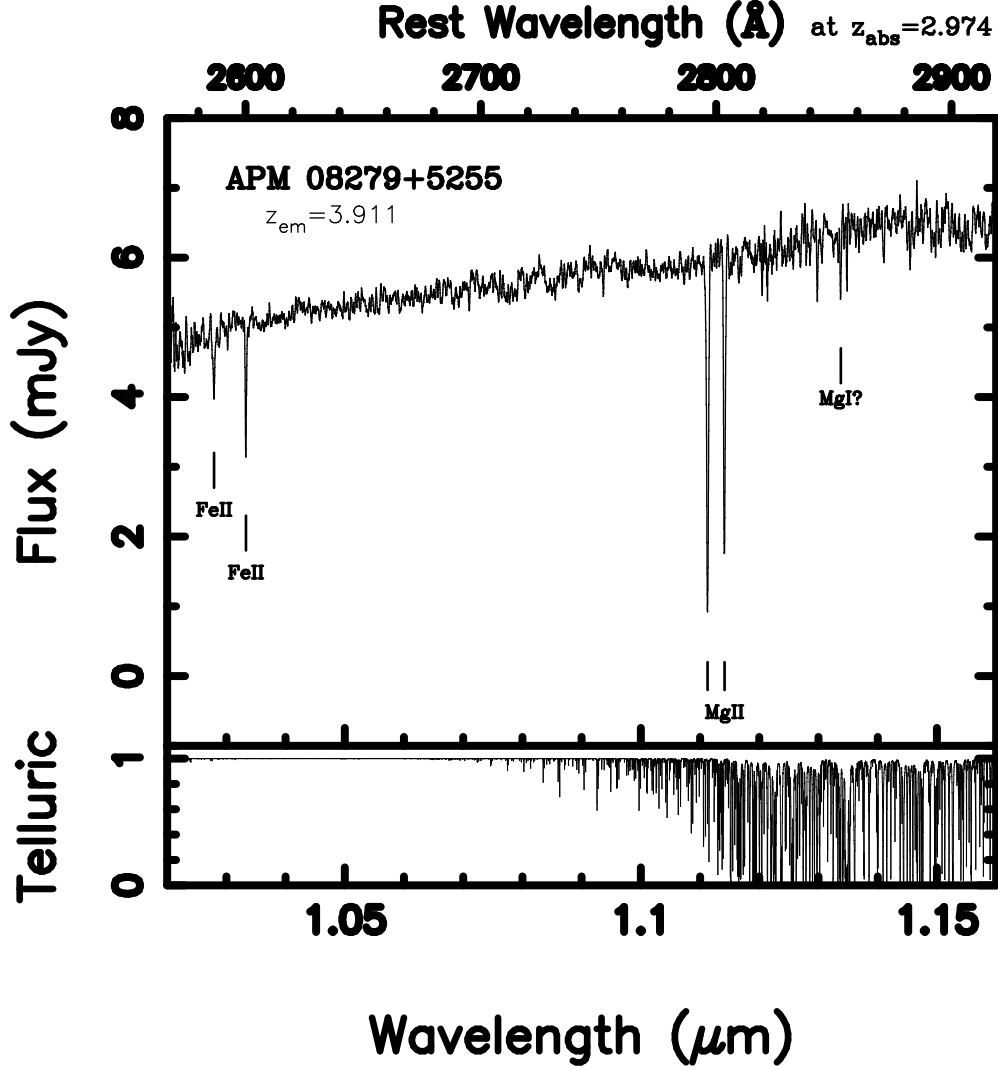
Wolfe, A. M. & Prochaska, J. X. 2000b, ApJ, 545, 591

Fig. 1.— The top figure shows $1.02 - 1.16 \, \mu$m spectrum of APM 08279+5255. All the frames of total integration time of 40 minutes were used to extract this spectrum. The horizontal axis shows the local-frame wavelength and the rest-frame wavelength at $z_{abs} = 2.974$ is shown at the top. The spectrum was smoothed with a 3-pixel (22.5 km s^{-1}) boxcar function. Mg II $\lambda\lambda$2796,2803, Fe II λ2600, Fe II λ2587 and probable Mg I λ2852 absorption lines from the DLA system are detected. The bottom figure shows the telluric absorption spectrum in the wavelength region calculated with ATRAN package software (Lord 1992).
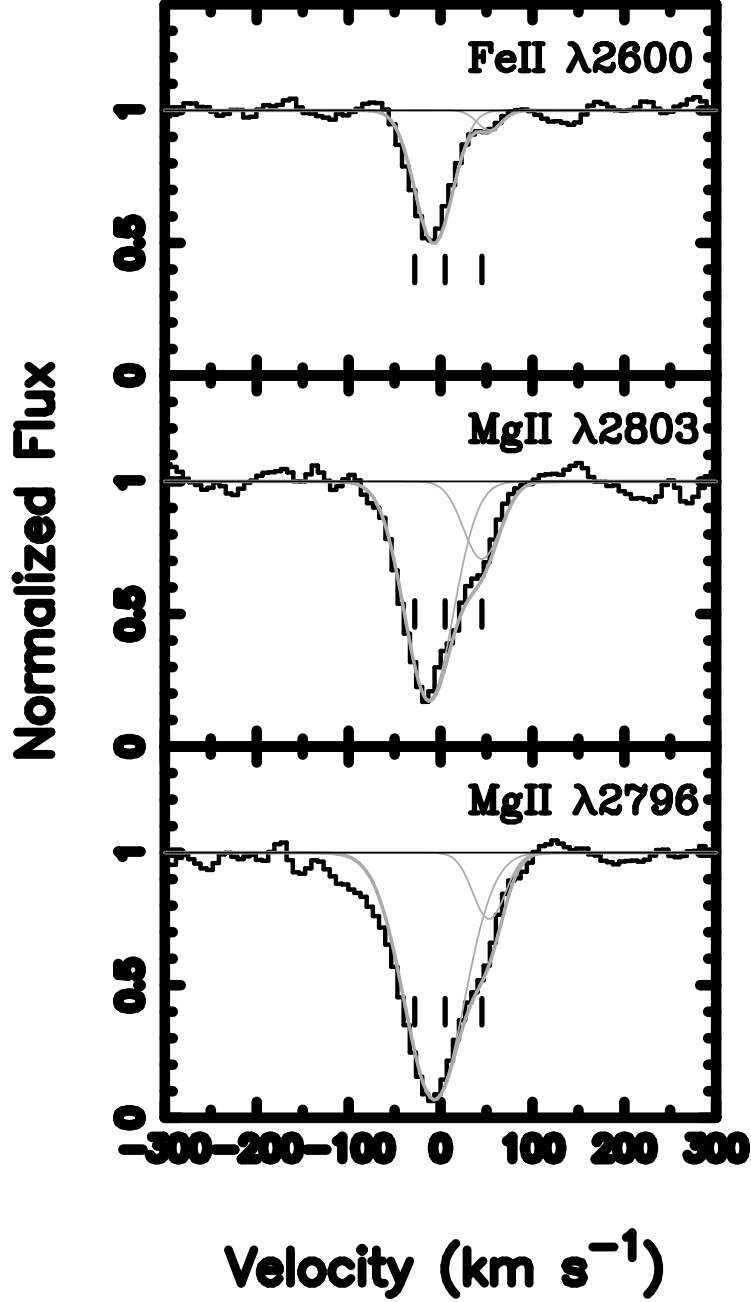
Fig. 2.— Velocity profile of Mg II $\lambda\lambda2796,2803$ and Fe II $\lambda2600$ absorption lines from the spectrum shown in Figure 1. Velocity resolution is about $40-45$ km s^{-1} ($\lambda/\Delta\lambda \sim 7000$). The locations of three velocity components (-28, +5, +45 km s^{-1}) from Petitjean et al. (2000) are marked with vertical tick marks. Because of insufficient spectral resolution, the -28 km s^{-1} and +5 km s^{-1} components are merged and show a single absorption peak at around -10 km s^{-1} ("main component"). The 45 km s^{-1} component is marginally resolved from the strong main component ("subcomponent"). The results of two-component Gaussian fitting (see text for detail) are shown with grey lines: thin grey lines show each Gaussian component and thick grey line shows the sum of the two components.
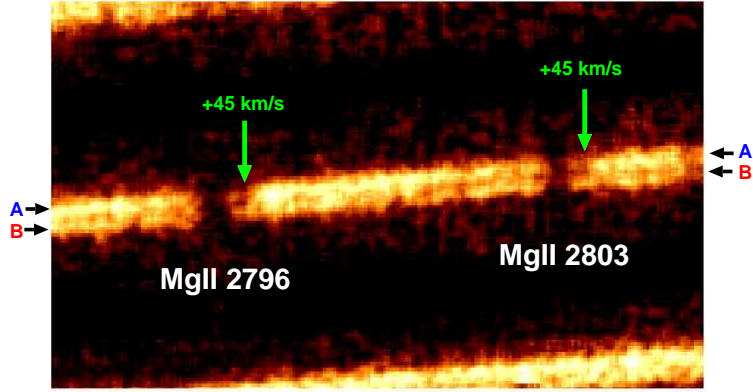
Fig. 3.— The echellogram of APM 08279+5255 centered at around $1.1125\,\mu$m, showing Mg II doublet absorption lines from the damped Lyman-α system at $z_{abs} = 2.974$. The image shown is from a frame with best seeing (frame No. 1, see Table 1) in which the QSO images A and B with $0\!''\!.38$ separation were most clearly resolved. The shown image was sky+dark subtracted (using the second frame), flat-fielded, then boxcared (3-pix$\sim$0$\!''\!.23$) for improving signal-to-noise. The absorption subcomponent at $+45$ km s^{-1} is marked. This subcomponent is seen in source A, but not in source B.
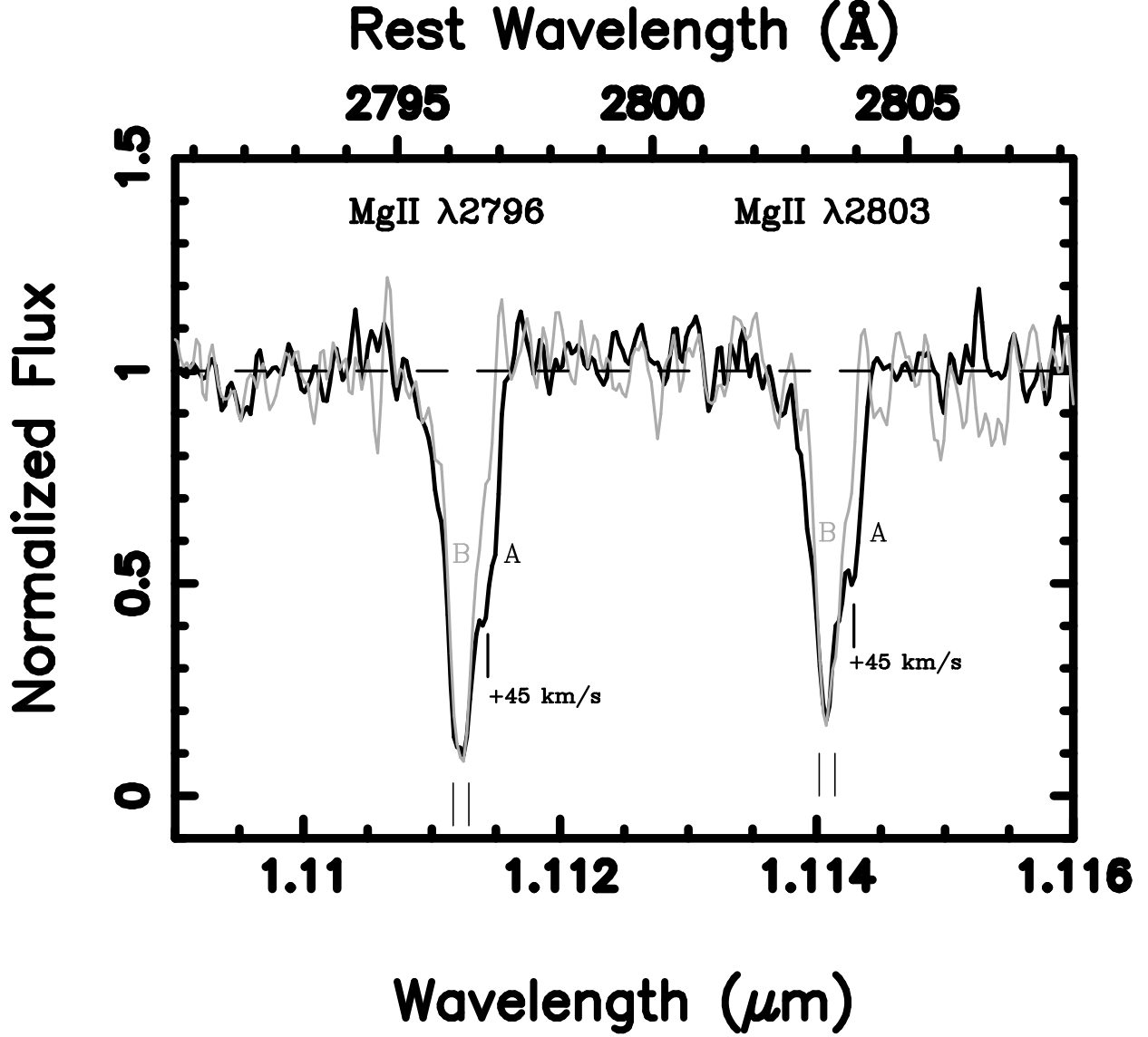
Fig. 4.— Extracted spectra of images A and B from a combined echellogram made from selected frames of good seeing (frames No.1-3, see Table 1). The horizontal axis shows the local-frame wavelength and the rest-frame wavelength at $z_{abs} = 2.974$ is shown at the top. The vertical axis is normalized flux to the continuum level. Black and grey line shows spectrum of source A and B, respectively. Three velocity components (-28, +5, +45 km s^{-1}) from Petitjean et al. (2000) are marked with thin tick marks. For both Mg II $\lambda2796$ and $\lambda2803$ lines, source A shows the subcomponent at +45 km s^{-1} while B does not. Because of less integration time, signal-to-noise is not as good as for the spectra in Figure 2. However, the subcomponent at 45 km s^{-1} is clearly detected in source A at more than 10σ.
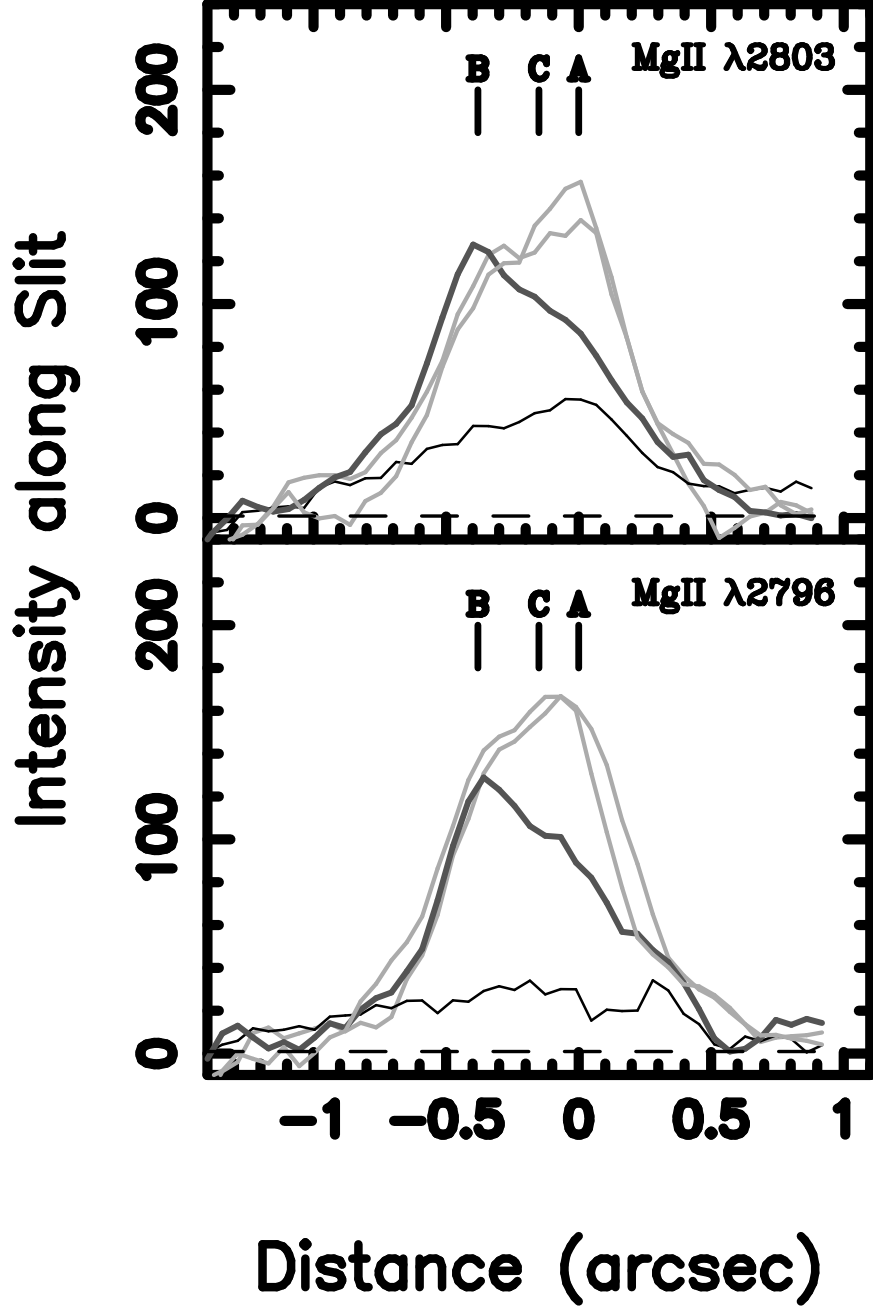
Fig. 5.— Spatial profile of the Mg II spectra from a combined echellogram made from selected frames of good seeing (frames No.1-3, see Table 1). The horizontal axis shows the distance from the peak of image A. The vertical axis shows the intensity in arbitrary unit. Dark grey, thin black, and light grey lines show the profile at the $+45$ km s^{-1} absorption component, at the bottom of the main absorption component, and the continuum on both short wavlength side and the long wavelength side of the absorption lines, respectively. Each profile was made by binning 4-pixels ($= 30$ km s^{-1}) in the spectrum direction. Four-pixel boxcar ($= 0\rlap{.}''3$) was applied in the spatial direction for improving signal-to-noise. The peak intensity of image B for the 45 km s^{-1} component (dark grey line) does not change from that for the continuum (light grey line). However, the peak intensity of image A for the 45 km s^{-1} component decreases significantly from the continuum level.
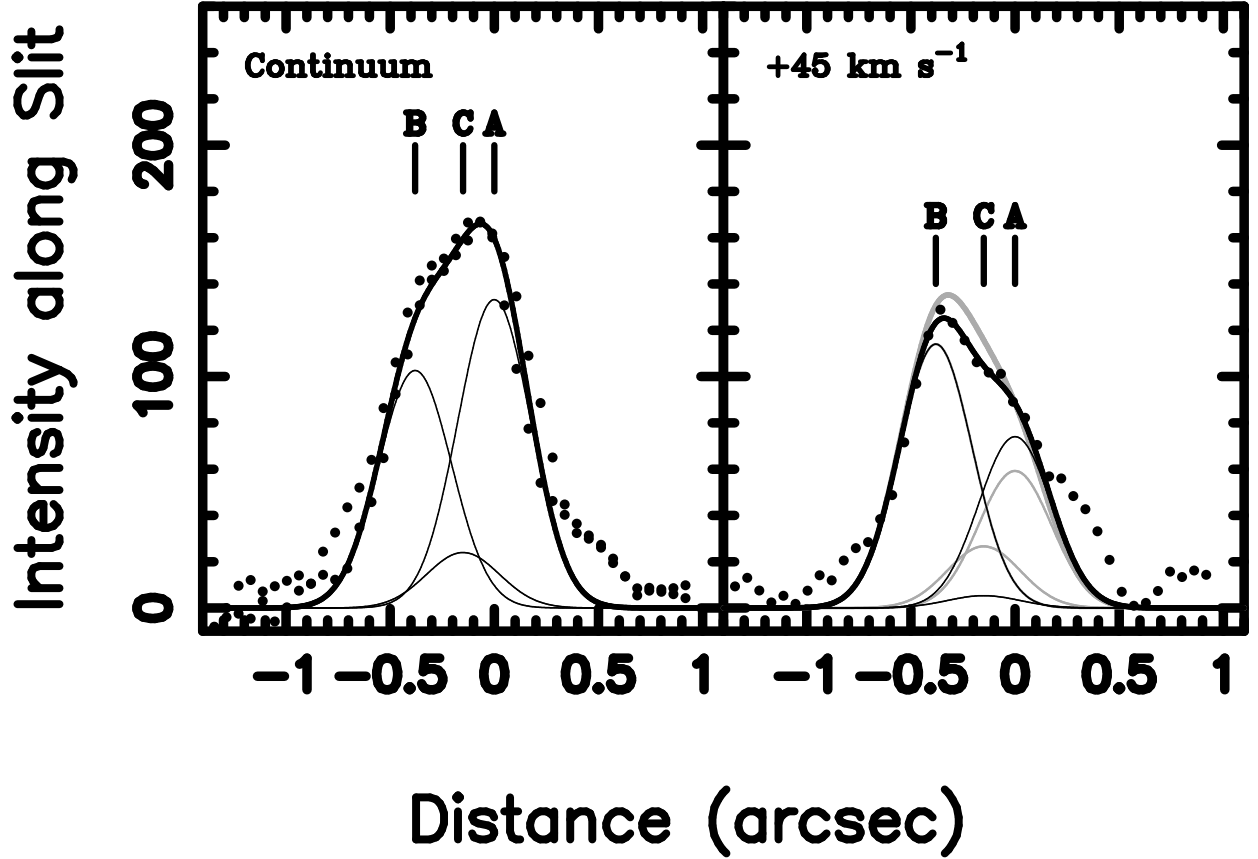
Fig. 6.— Three component gaussian fit to the spatial profiles in Figure 5. Black dots show the data points and the thick line shows the model fit. Thin lines show each gaussian component with peak at A, B, and C positions. The full-width-half-maximum of the gaussians is $0\rlap{.}''35$. The continuum profile (left) can be well fitted with three gaussian components with the flux ratio of the three images ($f_A : f_B : f_C = 1.30 : 1.00 : 0.23$) as in Ibata et al (1999). The profile at $+45$ km s^{-1} (right) was well fitted similarly with three gaussians with $f_A : f_B : f_C = 0.65 : 1.00 : 0.05$ (see black lines in the right panel). We tried to fit the $+45$ km s^{-1} profile with the same C flux as in the continuum profile, but could not reproduce the "dip" of the prifile at C-position well (grey lines show the fit with $f_A : f_B : f_C = 0.52 : 1.00 : 0.23$).

Table 1.   Observing Log for APM 08279+5255

Frame No.	Dither[a]	Time[b]	Integration time (sec)	Seeing[c] (arcsec)	Selection[d]
1	a	13:00	300	0.30	Yes
2	b	13:06	300	0.40	Yes
3	b	13:11	300	0.35	Yes
4	a	13:17	300	0.50	–
5	a	13:44	300	0.55	–
6	b	13:50	300	0.55	–
7	b	13:55	300	0.55	–
8	a	14:01	300	0.55	–

[a]Dithering positions of the object on the slit. Positions "a" and "b" have roughly $2''$ offset. Pairs of "a" and "b" was used for sky subtraction.

[b]UT time for exposure start. All data were obtained on 2001 Jan. 11 UT.

[c]Seeing in zJ band. Estimated from the FWHM of the spectra in the slit direction. Because the FWHM was estimated from profile fitting of A plus B assuming the separation of $0.''38$, the accuracy is not better than 1 pix ($\sim 0.''08$).

[d]Selected frames with good seeing. Frame No.1 was used for making Figure 3. Frames No.1-3 were used for making Figures 4, 5, and 6.

Table 2.   Absorption Lines in the System at $z_{abs} = 2.974$.

Species	Line	W_{obs}[a] (Å)	W_{rest}[b] (Å)	f[c]	Column Density[d] (cm^{-2})	log(X/H)[e]	log(X/H)$_\odot$[f]	[X/H][g]
Fe II	$\lambda 2587$	0.53	0.13	0.0684	13.5	-6.8	-4.49	-2.3
Fe II	$\lambda 2600$	0.97	0.24	0.2239	>13.3	>-7.0	-4.49	>-2.6
Mg II	$\lambda 2796$	3.44	0.87	0.6123	>13.3	>-7.0	-4.42	>-2.6
Mg II	$\lambda 2803$	2.46	0.62	0.3054	>13.5	>-6.8	-4.42	>-2.4
Mg I	$\lambda 2853$	0.29	0.07	1.81	11.7	-8.6	-4.42	-4.2

[a]W_{obs}: Total equivalent width in the observer frame. Typical uncertainty is 0.07Å.

[b]W_{rest}: Total equivalent width in the rest frame ($= W_{obs}/(1+z_{abs})$). Typical uncertainty is 0.02Å.

[c]Oscillator strength from Morton (1991) except for Fe II $\lambda 2587$ which is from Savage & Sembach (1996)

[d]See text for detail.

[e]Assuming log N(H) [cm^{-2}] = log N(H I) [cm^{-2}] = 20.3 (Petitjean et al. 2000)

[f]From Savage & Sembach (1996)

[g][X/H] = log(X/H) − log(X/H)$_\odot$

Table 3.   Velocity Components in Three Absorption Lines

Line	Rest Wavelength[a] (Å)	z	FWHM[b] (km s^{-1})	W$_{obs}$[c] (Å)	ID[d]
Fe II λ2600	2600.173	2.973909 $\pm$ 0.000012	48 $\pm$ 3	0.89 $\pm$ 0.04	main
		2.974709 $\pm$ 0.000093	31 $\pm$ 15	0.09 $\pm$ 0.03	sub
Mg II λ2796	2796.352	2.973913 $\pm$ 0.000012	76 $\pm$ 3	2.81 $\pm$ 0.08	main
		2.974703 $\pm$ 0.000030	41 $\pm$ 5	0.41 $\pm$ 0.07	sub
Mg II λ2803	2803.531	2.973835 $\pm$ 0.000015	62 $\pm$ 2	2.00 $\pm$ 0.07	main
		2.974598 $\pm$ 0.000037	47 $\pm$ 5	0.54 $\pm$ 0.07	sub

[a]From Morton (1991)

[b]Gaussian FWHM of the absorption line

[c]W$_{obs}$: Equivalent width in the observer frame

[d]Identification with the velocity components in Petitjean et al. (2000). "Main Component" is a combination of the systems spanning from -28 km s^{-1} to +5 km s^{-1} which cannot be resolved with the spectral resolution of the present data. "Subcomponent" is a subsystem at v = +45 km s^{-1}.